Supporting Information

Fiolka et al. 10.1073/pnas.1119262109

SI Text 1

To generate the necessary illumination patterns for SIM, an SLM is used as a programmable diffraction grating. By writing different pixel patterns to the SLM, the period, phase, and orientation of the illumination pattern can be modified. The following constraints need to be considered when designing such pixel patterns: in 3D SIM, the phase steps should evenly sample one pattern period in five steps. For best lateral resolution isotropy, the pattern needs to be rotated close to 60° for each orientation. To guarantee optimal resolution for different wavelengths and objectives, the period, and thus the diffraction angle, needs to be tunable in fine increments.

A further constraint is that the field of view is limited to the number of periods in the SLM pixel pattern multiplied by the period length at the sample space. Because most SLMs have fewer pixels than available cameras, it is therefore advantageous to design patterns with small pixel periods to allow illumination of a large field of view. However, small pixel periods lead to less tunability for the diffraction angle and the phase steps. To illustrate that point, consider a five-pixel pattern, as shown in Fig. S2*A*, that allows perfect 2π/5 phase steps in 3D SIM. Increasing the period by one pixel represents a 20% change, and the phase steps can no longer be close to the desired 2π/5.

Our approach to generate tunable pixel patterns with small pixel periods is as follows. The pixel pattern is constructed from a unit cell spanned by vectors $\vec{a} = (x_a, y_a)$ and $\vec{b} = (x_b, y_b)$ as shown in Fig. S2*B*. The main difference from previously used pixel patterns is that both vectors are allowed to be nonparallel to the axes. Vector $\vec{a}$ remains constant and defines the pattern orientation, whereas vector $\vec{b}$ is used to modify the pattern period.

With $\vec{n}$ being normal and equal in length to $\vec{a}$, the period, p, of the pattern equates to:

$$p = \vec{b} \cdot \frac{\vec{n}}{|\vec{n}|} = \frac{x_b y_a - y_b x_a}{\sqrt{x_a^2 + y_a^2}} \qquad \textbf{[S1]}$$

By changing vector $\vec{b}$ in pixilated steps, the numerator in equation Eq. **S1** can be set to any integer value. Thus, the period of the pattern can be any integer multiple of $1/|\vec{a}|$.

For a given set of vectors $\vec{a}$ and $\vec{b}$, the phase of the pattern can be adjusted by translating the unit cell in pixilated steps in x and y. The smallest phase step increment is inversely proportional to the area of the unit cell:

$$phasestep_{\min} = \frac{720^o}{|\vec{a}|p} \qquad \textbf{[S2]}$$

For the proposed pattern scheme, spurious diffraction orders will occur because of the coarsely pixilated stripes of the pattern. However, it can be shown that the spurious diffraction orders stay away from a line through the main diffraction orders in reciprocal space, as illustrated in Fig. 2*C*. The half-width of this line is $1/|\vec{a}|$. Thus, all unwanted diffraction orders can be blocked with a radial slot in a pupil plane, which has to be corotated for the three pattern orientations.

A large modulus of vector $\vec{a}$ allows fine-tuning of the period (which is important to match the diffraction angle) and the phase step (which is important to match the ideal phase steps closely), but it makes the filtering of the spurious diffraction orders harder. We found that setting the modulus of $\vec{a}$ to about 12 pixels represents a good compromise for patterns with periods as small as 4 pixels. For our setup, vector $\vec{a}$ was chosen as follows: $\vec{a_1} = (1, 12)$, $\vec{a_2} = (11, 5)$, $\vec{a_3} = (-10, 7)$. The orientation angle difference for the three resulting patterns equates to 60.79° and 59.77°, which is very close to the target value of 60°. The three vectors $\vec{a_1} \ldots \vec{a_3}$ remain unchanged, and the choice of vectors $\vec{b_1} \ldots \vec{b_3}$ tunes the pattern to the different imaging conditions. In Table S1, a choice for vectors $\vec{b_1} \ldots \vec{b_3}$ is given that allows optimal adaption of the pattern to the two laser lines and four Zeiss objectives that are integrated in our setup.

Two additional patterns are listed that allow one to operate the setup in TIRF SIM at two different penetration depths. The only necessary modification is a mask to block the zero-order beam and replacing the multimode fiber by a single mode fiber.

The smallest phase step increment for the shortest 3D SIM pattern is ~15°, which allows phase steps of 75° (close to the ideal 72° for 3D SIM).

The pixel pattern should have a ratio of "off" to "on" pixels of about 29% to adjust the center beam to about 70% of the intensity of the side beams. This requires a minimal period of four pixels to achieve similar on/off ratios. If the instrument were to be used in TIRF SIM mode only, this constraint would not exist because the zero-order center beam is blocked anyway. With our method, periods below three pixels are possible that would still allow for suitable phase stepping. Thereby, the demagnification of the SLM into the object plane can be reduced, and a larger field of view is illuminated.

SI Text 2

Base Medium. The base medium is prepared by mixing 2.5 g of glucose (41095; Acros), 500 mL of MEM [51200-038 (no phenol red); Invitrogen], 100 mg of $NaHCO_3$ (S-8875; Sigma), and 50 mg of transferrin (616420; Calbiochem).

Plating Medium. Five hundred milliliters of base medium is mixed with 50 mL of FBS (heat-inactivated at 57 °C for 30 min; SH30071.03HI; HyClone), 5 mL of 0.2-M L-glutamine solution (25030-081; GIBCO), 12.5 mg of insulin (I-6634 or I-1882; Sigma), and 5 mL of penicillin/streptavidin (15140-122; GIBCO).

GM. Five hundred milliliters of base medium is mixed with 25 mL of FBS, 1.25 mL of 0.2-M L-glutamine solution, 10 mL of B-27 supplement (17504-044; GIBCO), and 5 mL of penicillin/streptavidin.

Fig. S1. Resolution enhancement in 3D SIM. (*A*) Cross-section in Fourier space of the support, or the nonzero valued region, of the OTF in wide-field fluorescence microscopy. A microscope can collect the sample's spatial frequencies only from within this support, also known as the observable region that defines the resolution limit. The red dots represent the Fourier components of the illumination pattern used in 3D SIM. (*B*) Through frequency-mixing with the illumination components, the gray region of the sample's frequencies is made effectively observable; hence, resolution is extended by approximately a factor of two.

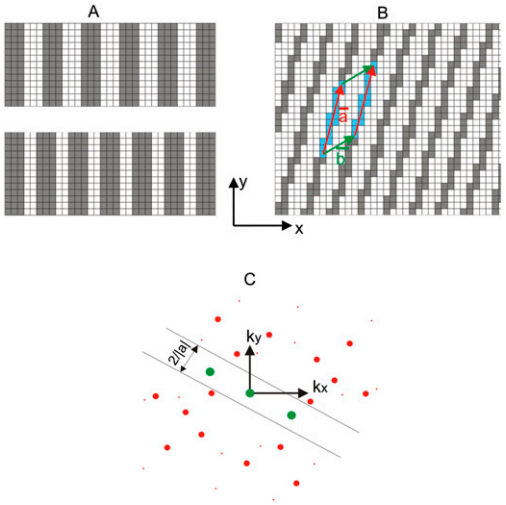

Fig. S2. Pattern generation for SIM. (*A*) Tuning the line spacing of a binary grating orientated along *x* from a five-pixel period to a six-pixel period ("on" pixels are shown in white, and "off" pixels are shown in gray). (*B*) Construction of a highly tunable pixel pattern. One unit cell is spanned by vectors $\vec{a}$ (red arrow) and $\vec{b}$ (green arrow), and the off pixels of that cell are rendered in light blue. Vector $\vec{a}$ determines the orientation of the pattern, whereas $\vec{b}$ is varied to tune the period of the pattern. (*C*) Schematic representation of diffraction orders in the pupil plane caused by the pixel pattern described in *B*. For a given vector $\vec{a}$, a strip along the zero and first diffraction orders (green dots) remains free of spurious diffraction orders (red dots) for any choice of vector $\vec{b}$. The width of that strip scales reciprocally with the magnitude of vector $\vec{a}$.

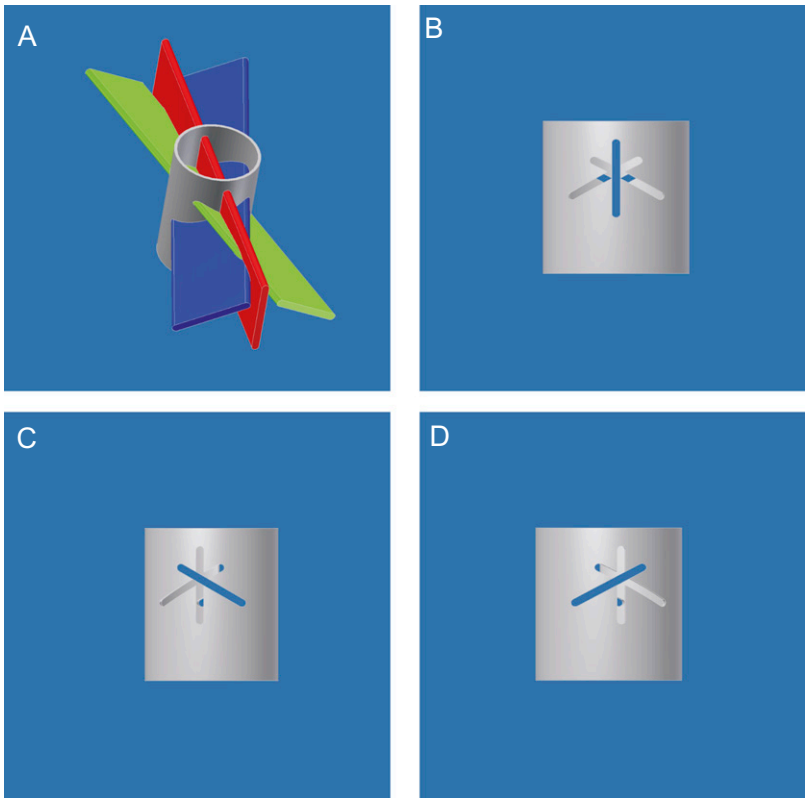

Fig. S3. Schematic illustration of the working principle of the rotating order selection mask. (*A*) The cylindrical mask is designed such that openings are made where three differently oriented planes (blue, red, and green) intersect it. (*B*) At the initial angular position of the cylinder, a slot for the first SIM pattern orientation is unobstructed, allowing the SIM beams to pass through. This process is repeated for the other orientations. (*C*) Slot for the second pattern orientation is cleared when the cylinder is rotated by −10°. (*D*) Slot for the third pattern orientation is cleared when the cylinder is rotated by 10°. The pairs of small holes that appear for each of the three cylinder orientations are blocked with an additional fixed mask.

Table S1. Optimized pixel pattern for 3D SIM using different objectives and for TIRF SIM at two different incident angles

Objective	$\overrightarrow{b_1}; \overrightarrow{b_2}; \overrightarrow{b_3}$	Period (pixel)	Pupil radius, %
N.A. = 1.4/magnification of 63×, oil, 488 nm	(4, 0);(3, −3);(−7, 0)	3.9–3.97	~91
561 nm	(−5, −6);(−2, 4);(−5, 9)	4.46–4.51	~91
N.A. = 1.2/magnification of 63×, water immersion, 488 nm	(−5, −3);(−7, 2);(−4, −3)	4.72–4.75	~88
561 nm	(−6, −7);(−2, 5);(2, −8)	5.38–5.4	~89
N.A. = 1.3/magnification of 63×, glyc. immersion, 488 nm	(−5, −9);(−3, −6);(−4, 8)	4.22–4.26	~91
561 nm	(−5, −1);(−3, 4);(0, 6)	4.88–4.92	~90
N.A. = 1.45/magnification of 100×, oil, TIRF, 488 nm	(−6, −2);(−3, 5);(3, 5)	5.79–5.82	~94
561 nm	(−6, 8);(−6, −10);(3, 6)	6.62–6.64	~95
N.A. = 1.45/magnification of 100×, oil, TIRF, 488 nm	(−6, −4);(−7, 3);(3, −9)	5.62–5.65	~97
561 nm	(−6, 6);(−2, −8);(3, −10)	6.45–6.47	~97

For each pattern, the vectors $\overrightarrow{b_1} \ldots \overrightarrow{b_3}$ for the three different orientations of the interference pattern are listed in the second column. The resulting pixel periods (minimum and maximum for $\overrightarrow{b_1} \ldots \overrightarrow{b_3}$) are shown in the third column. The radial position of the first-order diffraction spots in the pupil plane in our setup is listed in the last column. glyc, glycerol.

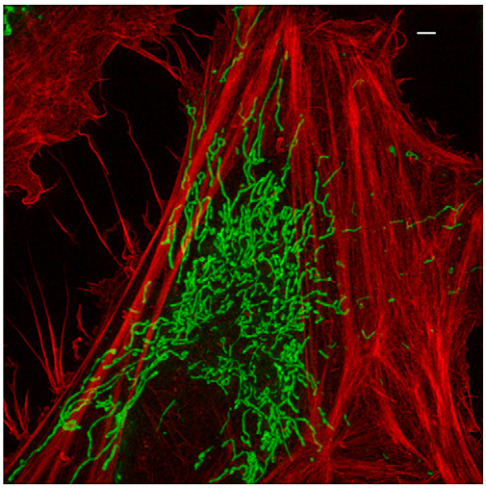

Movie S1. 3D SIM imaging of mitochondria labeled with MitoTracker green and the actin cytoskeleton labeled with tdTomato-LifeAct in a HeLa cell over 30 time points. The maximum intensity projection along the *z* axis through the entire volume is shown. Each time point (consisting of both color channels) was acquired within 22 s (20-ms raw exposure time). Mitochondria are rendered in green, and the actin cytoskeleton is rendered in red. (Scale bar: 2 μm.) The volume thickness is 3 μm.

Movie S1

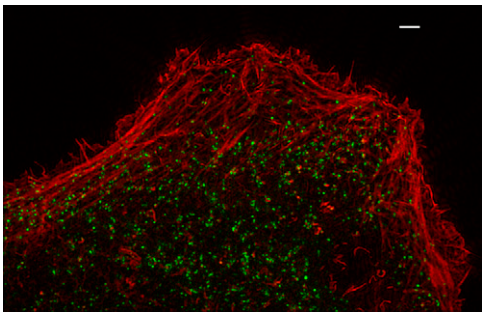

Movie S2. 3D SIM imaging of clathrin-coated vesicles labeled with mEmerald and the actin cytoskeleton labeled with tdTomato at the edge of a HeLa cell over 20 time points. The maximum intensity projection along the *z* axis through the entire volume is shown. Clathrin is rendered in green, and actin is rendered in red. Each time point (consisting of both color channels) was acquired within 8.5 s (20-ms raw exposure). (Scale bar: 2 μm.) The volume thickness is 1.25 μm.

Movie S2

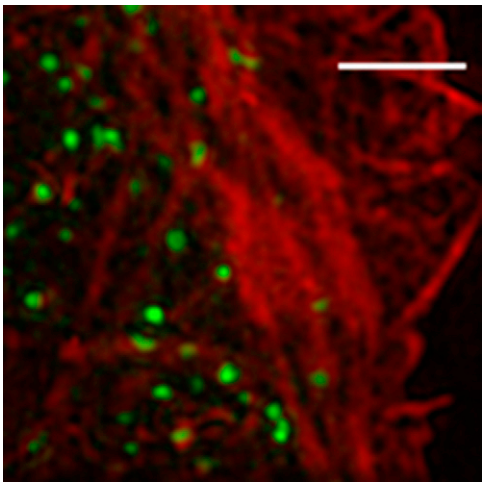

Movie S3. Enlarged subregion of Movie S2. Clathrin is rendered in green, and actin is rendered in red. The formation and disintegration (e.g., the only minimally moving green spot in the center) of a clathrin-coated vesicle can be observed. (Scale bar: 2 μm.) The volume thickness is 1.25 μm.

Movie S3

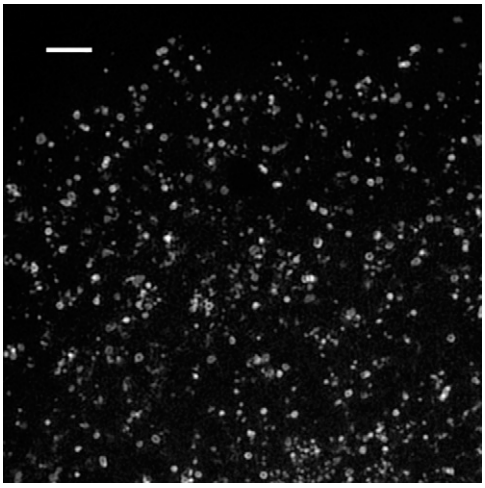

Movie S4. Dynamics of clathrin-coated vesicles labeled with mEmerald in another HeLa cell over 20 time points. The maximum intensity projection along the *z* axis through the entire volume is shown. Each data stack was acquired within 11.5 s (20-ms raw exposure), with an additional 13.5-s wait time inserted between the acquisition of data stacks. The formation of ring-shaped vesicles can be observed. (Scale bar: 2 μm.) The volume thickness is 3.625 μm.

Movie S4

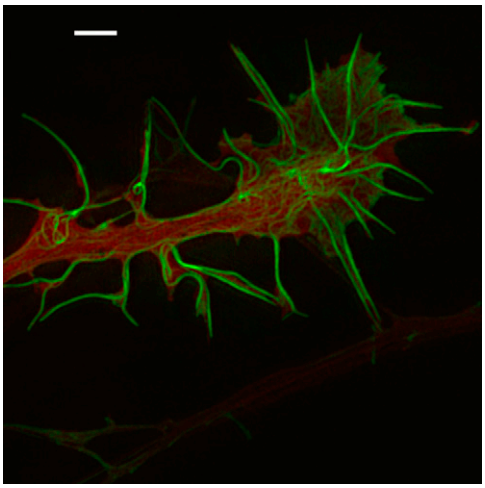

Movie S5. 3D SIM imaging of cultured neurons labeled with cytosolic GFP and actin labeled with td-Tomato over 20 time points. The maximum intensity projection along the *z* axis through the entire volume is shown. Each time point (consisting of both color channels) was acquired within 17 s (10-ms raw exposure time). The GFP channel is rendered in red, and actin is rendered in green (inverted compared with the other movies). (Scale bar: 2 μm.) The volume thickness is 3 μm.

Movie S5